Mechanism of effect of intrinsic defects on electrical and optical properties of Cu_2CdSnS_4: an experimental and first-principles study

2015 J. Phys. D: Appl. Phys. 48 445105

(http://iopscience.iop.org/0022-3727/48/44/445105)

IOP Publishing Journal of Physics D: Applied Physics
J. Phys. D: Appl. Phys. **48** (2015) 445105 (7pp) doi:10.1088/0022-3727/48/44/445105

Mechanism of effect of intrinsic defects on electrical and optical properties of Cu_2CdSnS_4: an experimental and first-principles study

Lei Meng[1], Yongfeng Li[1,2,5], Bin Yao[1,2,5], Zhan-Hui Ding[1], Gang Yang[1], Rui-Jian Liu[1], Rui Deng[3] and Lei Liu[4]

[1] State Key Lab of superhard material, and college of Physics, Jilin University, Changchun 130012, People's Republic of China
[2] Key Laboratory of Physics and Technology for Advanced Batteries (Ministry of Education), College of Physics, Jilin University, Changchun, 130012, People's Republic of China
[3] School of Materials Science and Engineering, Changchun University of Science and Technology, Changchun, 130022, People's Republic of China
[4] State Key Laboratory of Luminescence and Applications, Changchun Institute of Optics, Fine Mechanics and Physics, Chinese Academy of Sciences, Changchun 130033, People's Republic of China

E-mail: liyongfeng@jlu.edu.cn and binyao@jlu.edu.cn

Received 18 May 2015, revised 17 September 2015
Accepted for publication 18 September 2015
Published 9 October 2015

Abstract

Near stoichiometric and Cd-poor Cu_2CdSnS_4 (CCTS) thin films with p-type conductivity were prepared by magnetron sputtering and post-sulfurizing. It is found that the hole concentration of the Cd-poor CCTS is two orders of magnitude higher than that of the near stoichiometric CCTS while its optical bandgap is smaller than the near stoichiometric CCTS'. It is suggested by using first-principles calculations that the dominant intrinsic defects are Cu vacancy (V_{Cu}) and fully passivated defect complex of $2Cu_{Cd}+Sn_{Cd}$ in the Cd-poor CCTS, but V_{Cu} and Cu_{Cd} in the near stoichiometric CCTS. The V_{Cu} is responsible for the p-type conductivity of both CCTS films, while the $2Cu_{Cd}+Sn_{Cd}$ complex for smaller bandgap and higher hole concentration of the Cd-poor CCTS. The mechanism of effect of the intrinsic defects on the optical and electrical properties of the CCTS is suggested in the present paper.

Keywords: Cu_2CdSnS_4, thin film, magnetron sputtering, defect complex, first-principles calculation

(Some figures may appear in colour only in the online journal)

1. Introduction

Thin-film solar cells will make an increasingly important contribution to the next generation of solar devices as they can be manufactured with highly competitive costs. The highest photovoltaic conversion efficiency (PCE) of 20.8% has been reported for a thin-film $Cu(In,Ga)Se_2$ (CIGS) device [1]. However, there are concerns that the long-term production capacity could be hampered by price and availability of indium and gallium [2]. Thus, significant interests have been focused on finding new sustainable materials for solar devices. Cu_2MSnX_4 (M = Zn, Cd; X = S, Se) are considered as candidate materials [3–6], due to that the elements in the Cu_2MSnX_4 are abundant in the earth. In the recent years, a lot of research works are carried out on Cu_2ZnSnS_4 (CZTS) or $Cu_2ZnSn(S,Se)_4$ (CZTSSe). Many techniques or approaches have be used to prepare CZTS (or CZTSSe) thin film and CZTS-based thin film solar cell successfully, and

[5] Authors to whom any correspondence should be addressed.

the maximal efficiency of the CZTS-based thin film solar cell is 12.6% now [7]. However, some literatures reported about Cu_2CdSnS_4 (CCTS) or $Cu_2CdSn(S,Se)_4$ (CCTSSe) are few. Pan *et al* successfully synthesized CCTSSe film by a solution technique, with which CCTSSe-based solar cell with PCE of 3.1% was obtained [8]. In our previous work, a PCE of 1.2% was obtained in a $Cu_2Zn_{0.53}Cd_{0.47}SnS_4$-based solar cell [9]. Obviously, the PCE of the CCTS-based solar cell is much lower than that of the CZTS-based solar cell, that is mainly attributed to that the properties of the CCTS (CCTSSe) are not better than that of CZTS (CZTSSe). So, it is necessary to understand physical factors and related mechanisms of affecting properties of the CCTS (CCTSSe) films, in order to improve the PCE of the CCTS-based solar cell.

It is well known that properties of semiconductor are influenced by defects. It is reported that there are many types of intrinsic defects in CZTS (or CZTSSe), for example, antisite defects of Cu occupied Zn site (denoted as Cu_{Zn}) and Zn occupied Cu (Zn_{Cu}), Cu vacancies (V_{Cu}) [10–12] and passivated defect complex $[Cu_{Zn}+Zn_{Cu}]^0$. It has been demonstrated that the V_{Cu}, Zn_{Cu} and Cu_{Zn} defects determine the electrical properties of CZTS [10, 13], while the $[Cu_{Zn}+Zn_{Cu}]^0$ complex can affect the electron structure [14, 15], and that the intrinsic defects can be tuned by changing composition. Many literatures have been reported about intrinsic defects and their change with composition in CZTS film. The performance of CZTS-based solar cell also is improved by optimizing composition of CZTS, which tunes spices and amount of the intrinsic defects and so properties of the CZTS film. Therefore, it is important to understand spices of intrinsic defects in the absorber layer and their change with composition for improvement of PCE of solar cell. However, the information about intrinsic defects of CCTS is reported a little up to now.

In this paper, we comparatively investigated the electrical and optical properties of the near stoichiometric and Cd-poor CCTS thin films, and suggested intrinsic defects and influence of these defects on the properties of the CCTS by first-principles calculations.

2. Experimental and first-principles calculations details

The CCTS thin films were deposited on bare soda-lime glass (SLG) substrates by radio-frequency (rf) magnetron sputtering CCTS targets. Finely mixed Cu_2S, CdS, and SnS_2 powders with different molar ratios were pressed under 28 MPa at 700 °C for 30 min to form two ceramic CCTS targets and the purity of all the powders is 99.99%. One CCTS target has a near stoichiometric composition of Cu : Cd : Sn : S = 2 : 1 : 1 : 4 and the other has Cu : Cd : Sn : S = 2 : 2 : 1 : 4 (high Cd content target). The sputtering processes were carried out using 60 W rf power under 0.1 Pa working pressure with feeding Ar gas at a flow rate of 30 SCCM (standard cubic centimetre per minute). Before deposition, the target was pre-sputtered for 10 min to eliminate any contamination on its surface. Substrate temperature was fixed at 500 °C. The CCTS films produced by using the stoichiometric and high Cd content targets were denoted as C_2CTS_4 and $C_2C_2TS_4$, respectively.

Table 1. Composition analysis of the sulfurized CCTS thin films using EDS measurements.

Sample ID	Cu (at%)	Cd (at%)	Sn (at%)	S (at%)
C_2CTS_4	23.40	9.89	13.89	52.82
$C_2C_2TS_4$	23.44	12.52	13.01	51.03

After sputtering, the as-deposited CCTS thin films were put into a rapid thermal process (RTP) furnace together with sulfur powder and heated to 580 °C at a rapid heating rate of 5 °C. The temperature was kept 10 min and then set to cool down naturally to room temperature.

The surface images and composition of thin films were determined by a field emission scanning electron microscopy (FESEM) with an energy dispersive x-ray (EDS) analyser. Crystalline structure was analysed by x-ray diffraction (XRD) with Cu Kα radiation of 1.5406 Å. The electrical properties were investigated by a Hall Effect system in the Van der pauw configuration, the magnetic field scope was changed from 3 to 12 kG. Before Hall measurement, the ohmic contact of indium electrodes was confirmed using *I–V* measurement. The optical properties were measured using an UV–VIS–NIR spectrophotometer. All measurements were performed at room temperature.

First-principles calculations were performed using the VASP code with the projector augmented wave (PAW) potentials [16–19]. The calculations were performed using the hybrid functional as proposed by Heyd, Scuseria, and Ernzerhof (HSE) [20, 21]. For the Cu, Cd and Sn atoms, *d* electrons were treated as valence electrons. We constructed the 64-atom $2 \times 2 \times 1$ CCTS supercells with the kesterite structure. To simulate the CCTS with $2Cu_{Cd}+Sn_{Cd}$ defect complex, a Cd atom was replaced by a Sn atom and another two nearest-neighbour (NN) Cd atoms were also replaced by two Cu atoms. The cutoff energy for the plane-wave basis set was 500 eV. In the calculations, all the atoms were allowed to relax until the Hellmann – Feynman forces acting on them become less than 0.01 eV $Å^{-1}$.

3. Results and discussion

The chemical compositions of the sulfurized C_2CTS_4 and $C_2C_2TS_4$ thin films are listed in table 1. It is clear that the Cu, Sn and S contents in both films are almost constant, but the Cd content increases from 9.89 at% in the C_2CTS_4 to 12.52 at% in the $C_2C_2TS_4$, indicating that chemical ratio adjustment for the CCTS thin films can be realized by changing the target composition in sputtering and sulfurizing processes. The C_2CTS_4 is Cd-poor, and the $C_2C_2TS_4$ is near stoichiometric.

Figures 1(a) and (b) illustrate the x-ray diffraction (XRD) patterns of sulfurized C_2CTS_4 and $C_2C_2TS_4$ films, respectively. The XRD peaks are observed at 28.01°, 46.10°, 46.64° and 57.69° in figure 1(a), besides these peaks, a peak at 22.48° is also detected in figure 1(b), which are closed to the diffraction angles of (1 1 2), (2 2 0), (2 0 4), (2 2 4) and (1 1 0) planes of CCTS with kesterite structure, respectively [5, 6]. Some possible binary and ternary impurity phases such as $Cu_{2-x}S$, CdS and Cu_2SnS_3 are not detected in the films [22–25]. The enlarged (1 1 2) and (2 2 0)/(2 0 4) diffraction peaks of figures 1(a) and (b) are shown in figures 1(c) and (d),

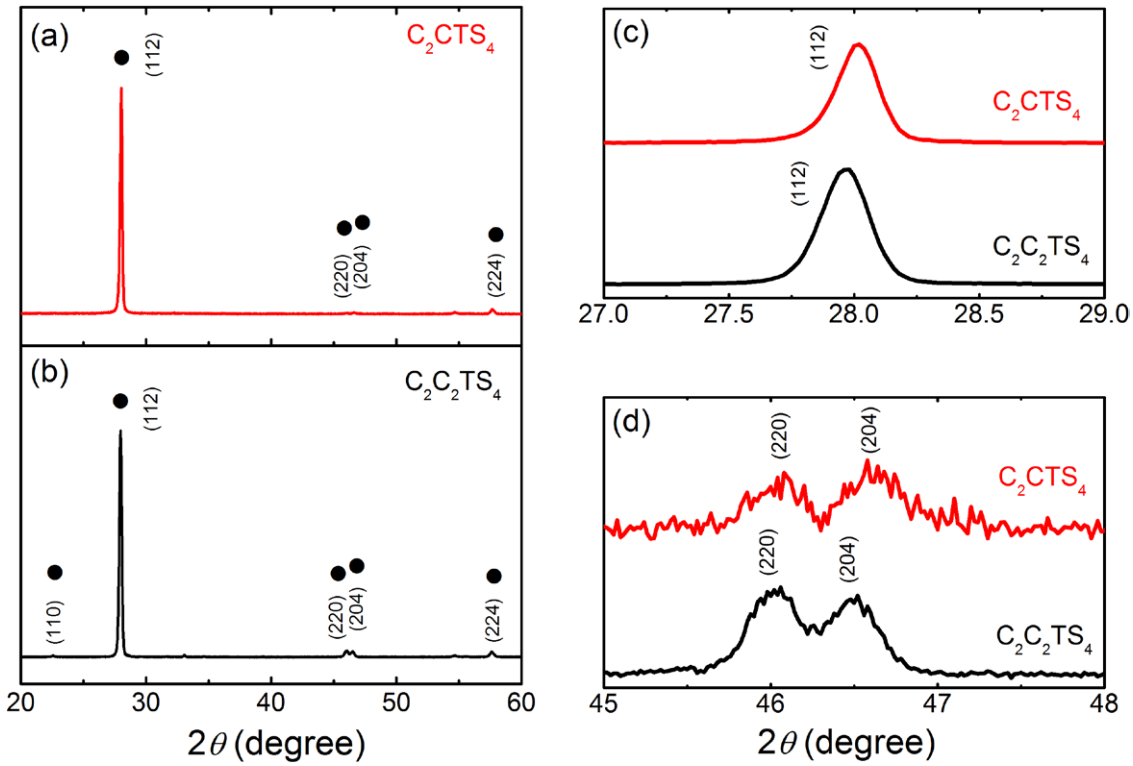

Figure 1. XRD patterns of the (a) Cd-poor and (b) near stoichiometric CCTS thin films deposited on SLG substrates. And the corresponding enlarged (c) (1 1 2), (d) (2 2 0) and (2 0 4) diffraction peaks in (a) and (b), respectively.

respectively. Comparing with the near stoichiometric CCTS thin film ($C_2C_2TS_4$), all the diffraction peaks of the Cd-poor CCTS (C_2CTS_4) thin film slightly shift towards direction with larger diffraction angle. The *a*- and *c*-axis lattice constants were calculated based on these XRD data. The *a*-axis lattice constant decreases from 0.558 nm of near stoichiometric CCTS to 0.546 nm of the Cd-poor CCTS, and the *c*-axis lattice constant decreases from 1.082 to 1.074 nm. the lattice constants of both CCTS are closed to those of kesterite CCTS structure [26].

Figures 2(a)–(d) show the surface SEM images of the as-deposited Cd-poor and near stoichiometric CCTS thin films by rf magnetron sputtering process, as well as these of the corresponding Cd-poor and near stoichiometric thin films after sulfurization. The insets in figures 2(a)–(d) show the corresponding cross-sectional images. The thickness of the films before and after annealing are 1.5 μm and 1.0 μm, respectively. The grain sizes are above 500 nm after sulfurizing, no pinholes or cracks were observed. Large grain sizes obtained by a rapid sulfurizing processing can reduce the grain boundaries. Figures 2(e) and (f) show the EDS spectra of both corresponding CCTS thin films, indicating that the thin films are composed of Cu, Cd, Sn and S elements and there are no characteristic peaks of the impurities in the CCTS thin films.

Combining with EDS analysis, we infer that the decrease in lattice constants may be due to following two reasons: one is increase of intrinsic defects induced by substitution of ion with smaller radius for ion with larger radius or generation of vacancies when the composition deviates from standard stoichiometric ratio, and the other is compressive strain [27], which usually make the optical bandgap of the film increase. However, it is found from the optical absorption spectra shown in figure 3 that the optical bandgap of the Cd-poor CCTS film does not increase but significantly decreases compared to that of the near stoichiometric CCTS, indicating that the decrease in lattice constants do not arise from the compressive stain but intrinsic defects. Furthermore, these intrinsic defects should be associated with the Cd-poor content in the C_2CTS_4 film.

The electrical properties of the sulfurized CCTS thin films were measured using the Hall Effect measurement system. Both the films exhibit p-type conductivity, and their carrier concentration, hall mobility and resistivity are listed in table 2. It is found that the Cd-poor CCTS film has a hole concentration of ~10^{18} cm^{-3}, two orders of magnitude higher than that of the near stoichiometric CCTS. It is well known that increase in hole concentration is attributed to increase in population of acceptor and/or decrease in transition energy of acceptor. Now the questions are as follows: (i) which kinds of acceptor defects contribute to p-type conductivity of the both CCTS films? (ii) How the population of the acceptor defect changes with the composition? And (iii) what factor results in decrease of transition energy. However, these questions are still not clear up to now.

In order to understand species of intrinsic defects and their effects on the properties of the CCTS, investigation about intrinsic defects and their effects on electronic structure was carried out based on first-principles calculations for the CCTS. As mentioned above, the both CCTS films show p-type conductivity, so they should have acceptor defects induced by substitution of Cu for Cd (Cu_{Cd}) and/or Cu vacancy (V_{Cu}), similar to CZTS, which is also p-type conductive, and its p-type conductivity is due to acceptor defects induced by substitution of Cu

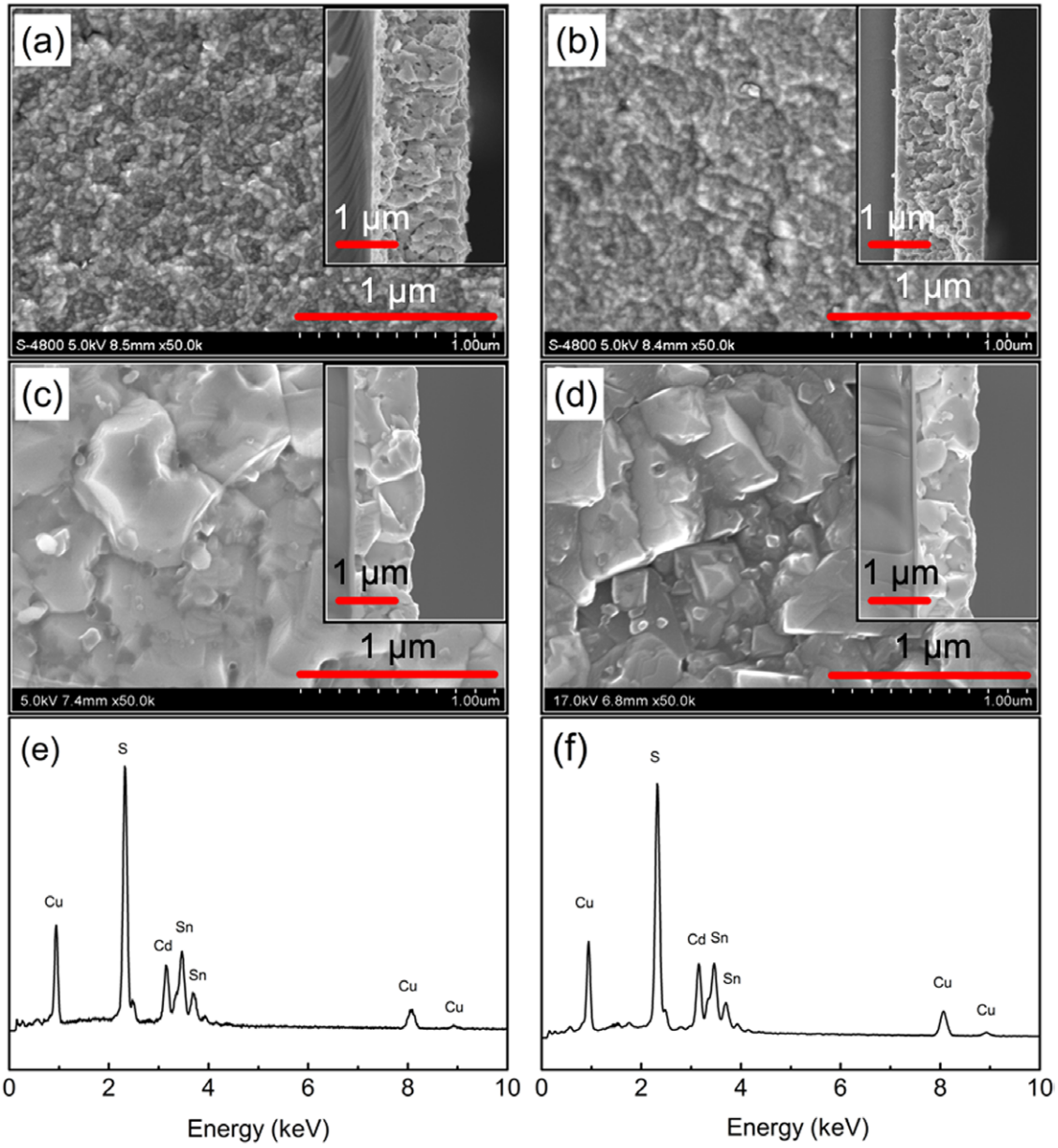

Figure 2. Surface SEM images of the as-deposited (a) Cd-poor and (b) near stoichiometric CCTS thin films by rf magnetron sputtering process, and those of the corresponding (c) Cd-poor and (d) near stoichiometric thin films after sulfurization. The EDS spectra of the sulfurized thin films (c) and (d) are shown in (e) and (f), respectively. The insets in (a)–(d) show the corresponding cross-sectional images.

for Zn site (Cu_{Zn}) and Cu vacancy (V_{Cu}) [14, 28–31]. In fact, since CCTS has similar crystalline and electronic structure to CZTS, it is reasonable to deduce that they may have similar intrinsic acceptor defects, such as Cu_{Cd} and V_{Cu}. In addition, as shown in table 1, the atomic ratio of Cd in the Cd-poor CCTS (9.89 at%) is much lower than that in standard stoichiometric CCTS (12.50 at%), while atomic ratio of Sn (13.89 at%) in the Cd-poor CCTS is higher than that (12.50 at%) in standard stoichiometric CCTS, so it is deduced that a Sn atom may occupy Cd site to form a donor defect (Sn_{Cd}), which may also bind with Cu_{Cd} acceptor defect to form an passivated defect complex, such as $2Cu_{Cd} + Sn_{Cd}$, due to coulomb interaction between donor and acceptor [32]. Based on above analysis, it is concluded that the intrinsic defects may include V_{Cu}, Cu_{Cd}, Sn_{Cd} and/or $2Cu_{Cd} + Sn_{Cd}$ complex in the Cd-poor CCTS.

In order to determined intrinsic defects in the Cd-poor CCTS, we first checked the stability of the $2Cu_{Cd} + Sn_{Cd}$ complex in CCTS. The binding energy of this complex can be expressed as

$$E_b = E_{tot}(2Cu_{Cd}+Sn_{Cd}) + 2E_{tot}(CCTS) - E_{tot}(Sn_{Cd}) - 2E_{tot}(Cu_{Cd}). \quad (1)$$

where E_{tot} is the total energy of the supercell system [33, 34]. A negative E_b indicates that the two defects tend to bind each other to form the complex. The calculated binding energy E_b for the $2Cu_{Cd}+Sn_{Cd}$ complex is 0.43 eV, indicating that the complex is stable with respect to the isolated Cu_{Cd} and Sn_{Cd} defects, that is, the Cu_{Cd} and Sn_{Cd} defects exist in a form of $2Cu_{Cd}+Sn_{Cd}$ complex in the Cd-poor CCTS. However,

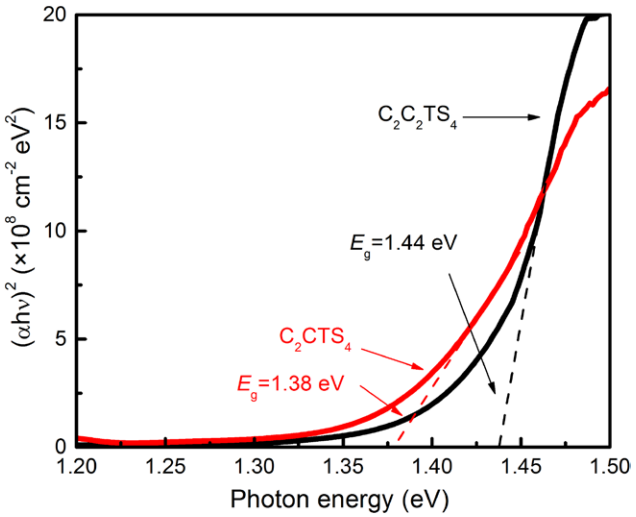

Figure 3. Optical absorption spectra of the Cd-poor and near stoichiometric CCTS thin films.

Table 2. Electrical properties of the sulfurized CCTS thin films.

Sample ID	Resistivity (Ω cm)	Carrier density(cm^{-3})	Hall mobility ($cm^2\ V^{-1}\ s^{-1}$)	Type
C_2CTS_4	6.5	1.1×10^{18}	7.8×10^{-1}	p
$C_2C_2TS_4$	2.9×10^2	3.5×10^{16}	1.7	P

$2Cu_{Cd}+Sn_{Cd}$ complex is charge-neutral and cannot contribute to hole concentration, so p-type conduction of the Cd-poor CCTS comes from contribution of the V_{Cu} acceptor. Based on the calculation and experimental results mentioned above, it is concluded that V_{Cu} and $2Cu_{Cd}+Sn_{Cd}$ complex are dominant intrinsic defects in the Cd-poor CCTS. Since Cd content is 12.52 at%, near atomic ratio of Cd in CCTS with standard stoichiometric ratio, it is hard to form Sn_{Cd} defect. So the intrinsic defects should be V_{Cu} and Cu_{Cd} in the near stoichiometric CCTS, as the same as CZTS with stoichiometric ratio.

Since Cd content in the Cd-poor CCTS is much lower than that in near stomchiometric CCTS, Cu_{Cd} and Sn_{Cd} form much easier in the Cd-poor CCTS than in the near stoichiometric CCTS, resulting in that the amount of $2Cu_{Cd}+Sn_{Cd}$ defects in the Cd-poor CCTS should be larger than the amount of Cu_{Cd} in the near stoichiometric CCTS. Owing to those radii of both Cu^{1+} (0.077 nm) and Sn^{4+} (0.069 nm) cations are smaller than that of Cd^{2+} (0.095 nm) cation, decrease in lattice constants induced by a $2Cu_{Cd} + Sn_{Cd}$ complex is larger than that induced by a Cu_{Cd}. Therefore, the lattice constants of *a* and *c* of the Cd-poor CCTS is smaller than that of the near stoichiometric CCTS, in agreement with XRD results shown in figure 1, confirming that the conclusions about the intrinsic defects in Cd-poor and near stoichiometric CCTS suggested by the first-principles calculations are correct. In addition, since the amount of Cu_{Cd} defects in the Cd-poor CCTS is larger than that of Cu_{Cd} in the near stoichiometric CCTS and Cu content is almost equal in both film, this result implies that the population of V_{Cu} in Cd-poor CCTS is larger than that in near stochiometric CCTS.

To well understand the observed bandgap narrowing of the Cd-poor CCTS film, we calculated the optical absorption

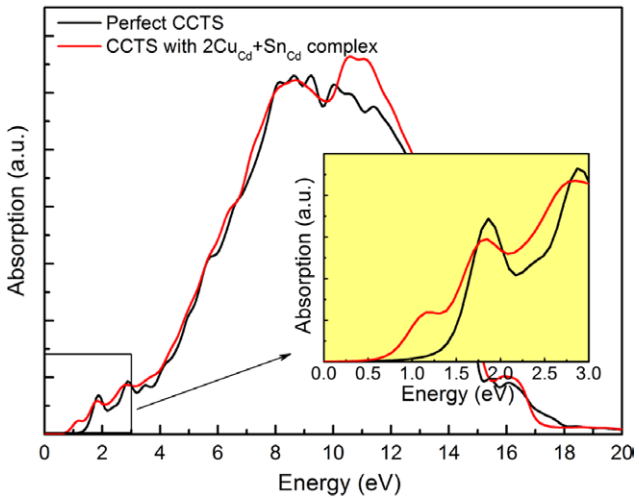

Figure 4. Calculated absorption spectra of the CCTS supercells with perfect structure and $2Cu_{Cd}+Sn_{Cd}$ complex. The inset shows an enlarged region near the band-edge of CCTS.

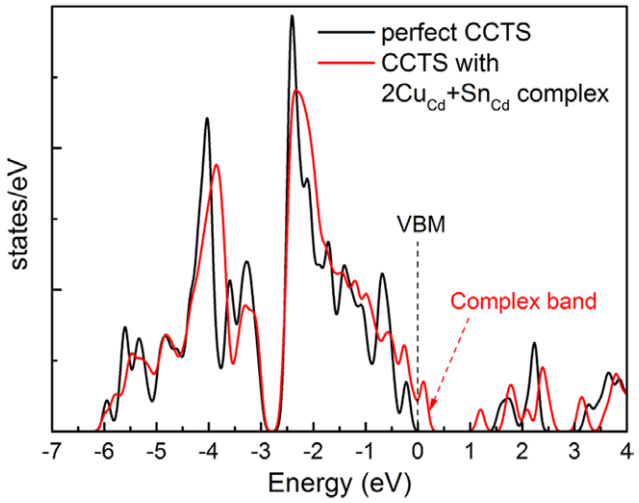

Figure 5. Total DOS of the CCTS supercells with perfect structure and $2Cu_{Cd}+Sn_{Cd}$ complex. The VBM is set to zero as energy reference.

spectra of the CCTS with perfect kesterite structure and $2Cu_{Cd}+Sn_{Cd}$ complex, as shown in figure 4. The inset of figure 4 shows an enlarged region near the band-edge of CCTS. The calculated absorption edge for the CCTS with $2Cu_{Cd}+Sn_{Cd}$ complex shows a significant red shift, compared to CCTS with perfect structure, consistent with the experimental results. Figure 5 shows the total density of state (DOS) of the CCTS without and with $2Cu_{Cd}+Sn_{Cd}$ complex. The valence-band maximum (VBM) is set as zero reference. Comparing with the perfect CCTS, the complex generates an additional fully occupied band above the VBM, resulting in increase in the level of the VBM. The electron transition will occur between conduction-band minimum (CBM) and the $2Cu_{Cd}+Sn_{Cd}$ occupied band as the photon with suitable energy is absorbed, leading to decrease in the optical bandgap measured.

It is speculated that the fully compensated band induced by $2Cu_{Cd}+Sn_{Cd}$ complex above VBM decreases equivalently

the transition energy of acceptor. To verify our speculation, we also calculated the transition energy $\varepsilon(0/-)$ of V_{Cu} in the CCTS supercell with perfect structure and $2Cu_{Cd}+Sn_{Cd}$ complex. Using the hybrid functional method, the calculated $\varepsilon(0/-)$ of the V_{Cu} in the CCTS without and with $2Cu_{Cd}+Sn_{Cd}$ complex is 0.22 and 0.09 eV, respectively. The transition energy of the V_{Cu} significantly decreases as the $2Cu_{Cd}+Sn_{Cd}$ complex is induced into the CCTS.

Based on discussed above, it is concluded that p-type conductivity of the CCTS comes mainly from contribution of V_{Cu} and the high hole concentration in the Cd-poor CCTS film is attributed to high population and low transition energy of V_{Cu}.

4. Conclusions

In summary, we prepared p-type the near stoichiometric and Cd-poor CCTS thin films with kesterite structure and investigated their structural, electrical and optical properties. With respect to the near stoichiometric CCTS film, the Cd-poor CCTS film shows smaller lattice constants, a higher hole concentration and the smaller bandgap. First-principles calculations suggest that the dominant intrinsic defects are V_{Cu} and $2Cu_{Cd}+Sn_{Cd}$ complex in the Cd-poor CCTS, but V_{Cu} and Cu_{Cd} in the near stoichiometric CCTS. The V_{Cu} is responsible for the p-type conductivity of both CCTS thin films, while the $2Cu_{Cd}+Sn_{Cd}$ complex for smaller bandgap and higher hole concentration of the Cd-poor CCTS, due to that the complex, on one hand, can increase the population of the V_{Cu}, on the other hand, can improve the level of the VBM and decrease transition energy of the V_{Cu} by generating an additional fully occupied band above the VBM. The improvement in the level of the VBM make the bandgap decrease, while decrease in the transition energy and increase in the population of V_{Cu} result in increase in hole concentration.

Acknowledgments

This work is supported by the National Natural Science Foundation of China under Grant Nos 10874178, 11074093, 61205038 and 11274135, Specialized Research Fund for the Doctoral Program of Higher Education under Grant No 20130061130011, PhD Programs Foundation of Ministry of Education of China under Grant No 20120061120011, Natural Science Foundation of Jilin province under grant No 201115013, and National Found for Fostering Talents of Basic Science under grant No J1103202. This work was also supported by High Performance Computing Center of Jilin University, China.

References

[1] Chirila A *et al* 2013 Potassium-induced surface modification of Cu(In,Ga)Se_2 thin films for high-efficiency solar cells *Nat. Mater.* **12** 1107–11
[2] Peter L M 2011 Towards sustainable photovoltaics: the search for new materials *Philos. Trans. R. Soc.* A **369** 1840–56
[3] Shin B, Gunawan O, Zhu Y, Bojarczuk N A, Chey S J and Guha S 2013 Thin film solar cell with 8.4% power conversion efficiency using an earth-abundant Cu_2ZnSnS_4 absorber *Prog. Photovolt.* **21** 72–6
[4] Xin H, Katahara J K, Braly I L and Hillhouse H W 2014 8% Efficient $Cu_2ZnSn(S,Se)_4$ solar cells from redox equilibrated simple precursors in DMSO *Adv. Energy Mater.* **4** 1301823
[5] Guan H, Zhao J C, Wang X and Yu F L 2013 Cu_2CdSnS_4 thin film prepared by a simple solution method *Chalcogenide Lett.* **10** 367–72
[6] Cao M, Li L, Fan W Z, Liu X Y, Sun Y and Shen Y 2012 Quaternary Cu_2CdSnS_4 nanoparticles synthesized by a simple solvothermal method *Chem. Phys. Lett.* **534** 34–7
[7] Wang W *et al* 2014 Device characteristics of CZTSSe thin-film solar cells with 12.6% efficiency *Adv. Energy Mater.* **4** 1301465
[8] Zhao W, Wang G, Tian Q, Huang L, Gao S and Pan D 2015 Solution-processed $Cu_2CdSn(S,Se)_4$ thin film solar cells *Sol. Energy Mater. Sol. Cells* **133** 15–20
[9] Xiao Z-Y *et al* 2013 Bandgap engineering of $Cu_2Cd_xZn_{1-x}SnS_4$ alloy for photovoltaic applications: a complementary experimental and first-principles study *J. Appl. Phys.* **114** 183506
[10] Chen S, Yang J-H, Gong XG, Walsh A and Wei S-H 2010 Intrinsic point defects and complexes in the quaternary kesterite semiconductor Cu_2ZnSnS_4 *Phys. Rev.* B **81** 245204
[11] Kosyak V, Mortazavi Amiri N B, Postnikov A V and Scarpulla M A 2013 Model of native point defect equilibrium in Cu_2ZnSnS_4 and application to one-zone annealing *J. Appl. Phys.* **114** 124501
[12] Nagaoka A, Miyake H, Taniyama T, Kakimoto K and Yoshino K 2013 Correlation between intrinsic defects and electrical properties in the high-quality Cu_2ZnSnS_4 single crystal *Appl. Phys. Lett.* **103** 112107
[13] Nagoya A, Asahi R, Wahl R and Kresse G 2010 Defect formation and phase stability of Cu_2ZnSnS_4 photovoltaic material *Phys. Rev.* B **81** 113202
[14] Chen S, Gong X G, Walsh A and Wei S-H 2010 Defect physics of the kesterite thin-film solar cell absorber Cu_2ZnSnS_4 *Appl. Phys. Lett.* **96** 021902
[15] Gokmen T, Gunawan O, Todorov T K and Mitzi D B 2013 Band tailing and efficiency limitation in kesterite solar cells *Appl. Phys. Lett.* **103** 103506
[16] Blöchl P E 1994 Projector augmented-wave method *Phys. Rev.* B **50** 17953–79
[17] Kresse G and Furthmüller J 1996 Efficient iterative schemes for *ab initio* total-energy calculations using a plane-wave basis set *Phys. Rev.* B **54** 11169–86
[18] Kresse G and Furthmüller J 1996 Efficiency of *ab initio* total energy calculations for metals and semiconductors using a plane-wave basis set *Comput. Mater. Sci.* **6** 15–50
[19] Kresse G and Joubert D 1999 From ultrasoft pseudopotentials to the projector augmented-wave method *Phys. Rev.* B **59** 1758–75
[20] Heyd J, Scuseria G E and Ernzerhof M 2003 Hybrid functionals based on a screened Coulomb potential *J. Chem. Phys.* **118** 8207–15
[21] Heyd J, Scuseria G E and Ernzerhof M 2006 Erratum: 'Hybrid functionals based on a screened Coulomb potential' [*J. Chem. Phys.* **118**, 8207 (2003)] *J. Chem. Phys.* **124** 219906
[22] Seboui Z, Cuminal Y and Kamoun-Turki N 2013 Physical properties of Cu_2ZnSnS_4 thin films deposited by spray pyrolysis technique *J. Renew. Sustain. Energy* **5** 023113
[23] Narayana T, Subbaiah Y P V, Prathap P, Reddy Y B K and Reddy K T R 2013 Influence of sulfurization temperature on physical properties of Cu_2ZnSnS_4 thin films *J. Renew. Sustain. Energy* **5** 031606

[24] Vigil-Galan O, Courel M, Espindola-Rodriguez M, Izquierdo-Roca V, Saucedo E and Fairbrother A 2013 Toward a high Cu_2ZnSnS_4 solar cell efficiency processed by spray pyrolysis method *J. Renew. Sustain. Energy* **5** 053137

[25] Pani B and Singh U P 2013 Preparation of Cu_2ZnSnS_4 thin film by a simple and cost effective route using metallic precursors and effect of selenization on these films *J. Renew. Sustain. Energy* **5** 053131

[26] Ionkin A S, Fish B M, Marshall W J and Senigo R H 2012 Use of inorganic fluxes to control morphology and purity of crystalline késterite and related quaternary chalcogenides *Sol. Energy Mater. Sol. Cells* **104** 23–31

[27] Li C R *et al* 2013 Electronic and optical properties of kesterite Cu_2ZnSnS_4 under in-plane biaxial strains: first-principles calculations *Phys. Lett.* A **377** 2398–402

[28] Mendis B G *et al* 2014 Direct observation of Cu, Zn cation disorder in Cu_2ZnSnS_4 solar cell absorber material using aberration corrected scanning transmission electron microscopy *Prog. Photovolt.* **22** 24–34

[29] Maeda T, Nakamura S and Wada T 2011 First principles calculations of defect formation in in-free photovoltaic semiconductors Cu_2ZnSnS_4 and $Cu_2ZnSnSe_4$ *Japan. J. Appl. Phys.* **50** 04DP07

[30] Chen S, Walsh A, Gong X G and Wei S H 2013 Classification of lattice defects in the kesterite Cu_2ZnSnS_4 and $Cu_2ZnSnSe_4$ earth-abundant solar cell absorbers *Adv. Mater.* **25** 1522–39

[31] Han D *et al* 2013 Deep electron traps and origin of p-type conductivity in the earth-abundant solar-cell material Cu_2ZnSnS_4 *Phys. Rev.* B **87** 155206

[32] Chen S Y, Wang L W, Walsh A, Gong X G and Wei S H 2012 Abundance of $Cu_{Zn} + Sn_{Zn}$ and $2Cu_{Zn}+Sn_{Zn}$ defect clusters in kesterite solar cells *Appl. Phys. Lett.* **101** 223901

[33] Zhou H *et al* 2014 Wavelength-tuned light emission via modifying the band edge symmetry: doped SnO_2 as an example *J. Phys. Chem.* C **118** 6365–71

[34] Li YF, Deng R, Tian YF, Yao B and Wu T 2012 Role of donor-acceptor complexes and impurity band in stabilizing ferromagnetic order in Cu-doped SnO_2 thin films *Appl. Phys. Lett.* **100** 172402